

Structural, Dielectric and Magnetic Behavior of Cu²⁺ Substituted Ni-Zn Ferrite by Auto-combustion Technique.

V.V.Awati^{*}, D. H. Bobade^{*}, Mrs S. D. Kulkarni^{**}, S.M.Rathod^{***}

^{*}Research scholar, JJT University, Jhunjhunu, Rajasthan, India

Department of Physics, C. T. Bora College, Shirur, Dist. Pune, India

^{**}Scientist CMC, National Chemical Laboratory, Pune, India

^{***}P. G. & Research, Department of Physics, Abasaheb Garware College, Pune-411004, India

ABSTRACT

Structural and magnetic properties of Cu²⁺ substituted Ni_{0.8-x}Cu_xZn_{0.2}Fe₂O₄ ferrites for x = 0.0 to 0.6 with the step increment of 0.2 prepared by an auto-combustion method have been investigated. The X-ray diffraction pattern of these compositions confirmed the formation of the single phase spinel structure. Further, the XRD have been used to calculate the lattice parameter and grain size. The particle size of the starting powder composition varied from 25 nm to 40 nm. The morphological investigations and nanometric sizes of the samples was studied by using scanning electron microscopy and transmission electron microscopic techniques. Dielectric constant varied from 75 to 3000 with frequency, rise in copper concentration and temperature. All the samples follow the Maxwell-Wagner's interfacial polarization. Saturation magnetization decreased from 152.15 emu/g to 42.05 emu/g for as burnt samples and from 48.63 emu/g to 43.368 emu/g for samples sintered at 700° C. The influence of Cu substituent on Ni-Zn ferrite is investigated by UV measurement at room temperature and at 700° C. These nanoferrites may have application in core materials and in electronic device technology.

Keywords: Auto-combustion, Dielectric Constant, Ferrites, Nanocrystalline Magnetic materials.

I. INTRODUCTION

Soft ferrites are the most widely used magnetic materials having low cost, high performance for high-frequency applications. Ni-Zn ferrites have many important applications in this context. The properties of ferrites are also very sensitive to the processing techniques and particle size. With the improvement in the synthesis and characterization techniques to the nanoscale, there is tremendous growth in the field of ferrites. Superparamagnetism, spin canting, core-shell structure, metastable cation distribution etc are some of the phenomena, which have been observed in various nanoferrites. These phenomena depend on number of factors such as composition, grain size, surface morphology, anisotropy, interparticle

interactions [1]. The synthesis and characterization of superparamagnetic nanoparticles of spinel ferrites with the chemical formula MFe₂O₄ (M=Co,Cu Mn, Ni, Zn, Mg etc) have been investigated with much interest [2, 3, 4]. Ferrite nanocrystals are also of interest in various applications, such as inter-body drug delivery [5-7], bioseparation, and magnetic refrigeration systems [8], as they exhibit superparamagnetism [9]. In addition, among ferrosinels Cu substituted ferrites are used in gas sensing [10-11], catalytic application [12], photocatalyst [13-14], and absorbent materials [15]. Doping ferrite nanocrystals with various metals usually improve some of their electric or magnetic properties [16-18]. For example Ni-Zn ferrites have applications as soft magnetic materials with high frequency (due to high electrical resistivity and low eddy-current loss [19]). Along that line Ni-Cu-Zn ferrites offer a further improvement as softer magnetic materials [20]. The purpose of this research is to investigate the role of Cu substitution on structural, dielectric and magnetic properties on Ni-Zn ferrites through sol-gel method. Specially, we characterize structural and magnetic properties of the doped samples at room temperature and for the samples sintered at 700° C. The various techniques are employed such as x-ray diffraction (XRD), Field-Emission Scanning Electron Microscope (FE-SEM), Fourier Transform Infra-Red (FTIR) spectroscopy, Vibrating Sample Magnetometer (VSM) and UV-Vis spectrometer at room temperature. The successful experimental approach will open a new gateway for improving devices based on NiCuZn ferrites, which are used in the surface mount devices (SMD) and multilayer chip inductors (MLCI) due to their high electrical resistivity and soft magnetic properties at high frequencies. These devices are used in electronic applications such as telecommunication. The efficiency of these devices is strongly dependent on the structural, electrical and magnetic properties of the materials. The systematic research is still necessary for a more comprehensive understanding and properties of such materials.

2. Experimental

2.1 Synthesis of Nanoferrites

$\text{Ni}_{0.8-x}\text{Cu}_x\text{Zn}_{0.2}\text{Fe}_2\text{O}_4$ (where $x = 0.0, 0.2, 0.4, 0.6$) nanoferrites were prepared by sol-gel method. The precursor solution was prepared using AR grade metal nitrates; $\text{Cu}(\text{NO}_3)_2$, $\text{Zn}(\text{NO}_3)_2$, $\text{Ni}(\text{NO}_3)_2$, and $\text{Fe}_2(\text{NO}_3)_2$. These nitrates were initially dissolved separately in distilled water and stirred well for 20 minutes at 80°C , subsequently the precursor solution was prepared by adding all above solutions and continuously stirred for 30 minutes at 80°C . An aqueous solution of citric acid mixed with metal nitrate solution, then ammonia solution was slowly added to adjust the pH at 7. The mixed solution was kept on to a hot plate with continuous stirring at 100°C . When finally all water molecules were removed from the mixture, the viscous gel began frothing. After few minutes the gel automatically ignited and burns with glowing flints. The auto combustion was completed within a minute, yielding a brown colored ashes termed as precursor. The as prepared powders were sintered at 400°C & 700°C for two hours to get the final product. Also the prepared ferrite mass was pressed in the form of pellets of 10 mm diameter with the help of hydraulic press by applying pressure of 60 kg/cm^2 for 1-2 minute. These pellets were sintered at 400°C for two hours in air medium.

2.2. Characterization

Powder X-ray diffraction (XRD) pattern was carried out on a X-ray diffractometer (Model Bruker D8), with $\text{CuK}\alpha$ irradiation ($\lambda = 1.5405\text{ \AA}$). The lattice parameter, crystallite (grain) size of the prepared samples were calculated from the XRD data. The Scanning Electron Microscope (SEM) JEOL JSM-6360A and Transmission Electron Microscope PHILIPS (Model CM 200) was used to study the morphology and to estimate grain size. The dielectric constant, loss factor ($\tan \delta$) was measured by two probe method using precision LCR meter bridge (HP 4284 A) in the frequency range of 100 Hz to 1 MHz at room temperature. Vibrating Sample Magnetometer (VSM) was employed to study the magnetic properties of the samples in the field of 5 kOe at room temperature.

3. Results and Discussions

3.1 Structural Analysis

Fig. 1(a) and Fig. 1(b) shows XRD pattern of as burnt and samples sintered at 700°C of $\text{Ni}_{0.8-x}\text{Cu}_x\text{Zn}_{0.2}\text{Fe}_2\text{O}_4$ ferrites for $x = 0.0$ to 0.6 with the step increment of 0.2 prepared by sol-gel method. These diffraction peaks give the evidence of the formation of ferrite phase in all samples. The peak position and relative intensity of all diffraction peaks match well with the standard powder diffraction file of JCPDS [21].

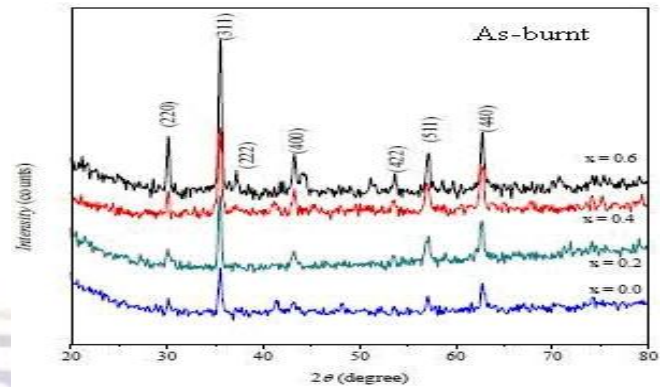


Fig 1(a) : XRD pattern of as burnt samples of $\text{Ni}_{0.8-x}\text{Cu}_x\text{Zn}_{0.2}\text{Fe}_2\text{O}_4$.

Furthermore, no impurity peaks or secondary phases were observed which indicates that the formation of high purity crystalline $\text{Ni}_{0.8-x}\text{Cu}_x\text{Zn}_{0.2}\text{Fe}_2\text{O}_4$ ferrites for $x = 0.0$ to 0.6 with the step increment of 0.2 . Further, it is observed from fig. 1, for the as burnt samples (fig. 1(a)), the reflection are relatively weak, indicating its low crystallinity and small particle size. The average particle size for each composition was calculated from the (311) plane using Scherrer formula [22].

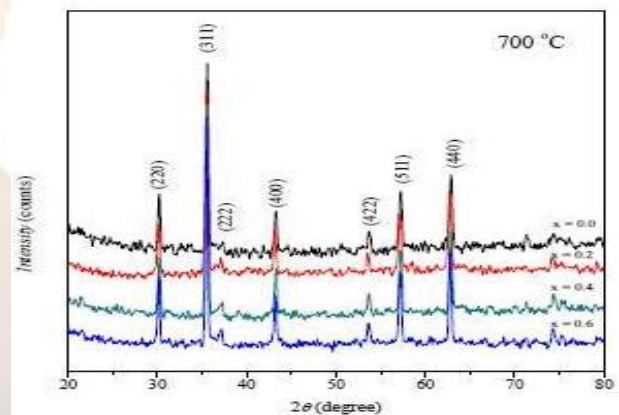


Fig. 1(b) XRD pattern of the samples sintered at 700°C of $\text{Ni}_{0.8-x}\text{Cu}_x\text{Zn}_{0.2}\text{Fe}_2\text{O}_4$

Upon substitution of Cu^{2+} ions, the lattice parameter was found to increase with increasing concentration of substituted ions as shown in Fig. 2. This change in lattice parameter was expected as the ionic radius of Cu^{2+} ions (0.73 \AA) is greater than the ionic radius of Ni ions (0.69 \AA) [23]. The observed lattice parameter and specific indices are characteristic of spinel structure confirms the formation of cubic spinel structure in ferrite [24-27]. The patterns do not show any unidentified peaks confirming no diffusion or any chemical reaction during sintering as shown in Fig. 1(b) [28].

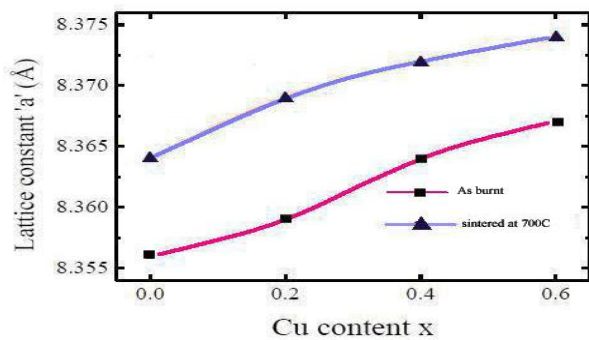


Fig. 2 : Variation of lattice parameters with copper content(x) for various $Ni_{0.8-x}Cu_xZn_{0.2}Fe_2O_4$

Fig. 3 shows that crystallite sizes are in the range of nanometer and exhibit gradual increase with the increasing in Cu^{2+} content. The size of the particle is observed to be increased with increase in sintering temperature. While sintering generally decreases the lattice defects and strains, however it can also cause coalescence of crystallites that result in increasing the average size of the nanoparticles [29]. Fig. 3 also shows the dependence of particle size on sintering temperature and Cu^{2+} substitution. Thus it appears that particle size may be controlled by varying sintering temperature.

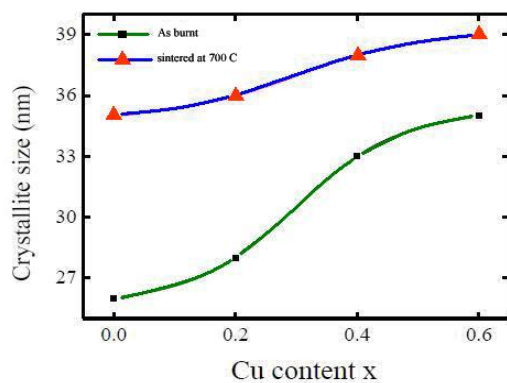


Fig.3 : Variation of crystallite size with Cu content x for as burnt and the samples sintered at $700^{\circ}C$

3.2 Scanning Electron Microscopy (SEM)

Microstructural analysis determines the average grain size and the type of grain growth of the samples, which influence the magnetic properties of the materials. The SEM micrographs of various $(Ni_{0.8-x}Cu_xZn_{0.2})Fe_2O_4$ samples as prepared and sintered at $700^{\circ}C$ are shown in fig.4. Average grain sizes of the samples are determined from these micrographs. The average grain sizes of the samples increases due to the substitution of Cu^{2+} . This increase in grain size may be attributed to the higher atomic mobility of Cu ions as reported by Dimri et. al, [30,31]. This may be due to the fact that the melting point of copper (1357 K) is less than that of

nickel (1726 K). This result agrees with the result for Zn^{2+} , Cd^{2+} , Ti^{4+} substituted ferrites [32, 33]. At low composition, formation of large exaggerated grains of non-uniform size is seen to occur. The driving force for grain growth is the surface tension of the grain boundary [34].

Figure 4 also shows the difference between the grain size related to the different sintering temperature. The size of the grains is observed to be increased with sintering temperature [35].

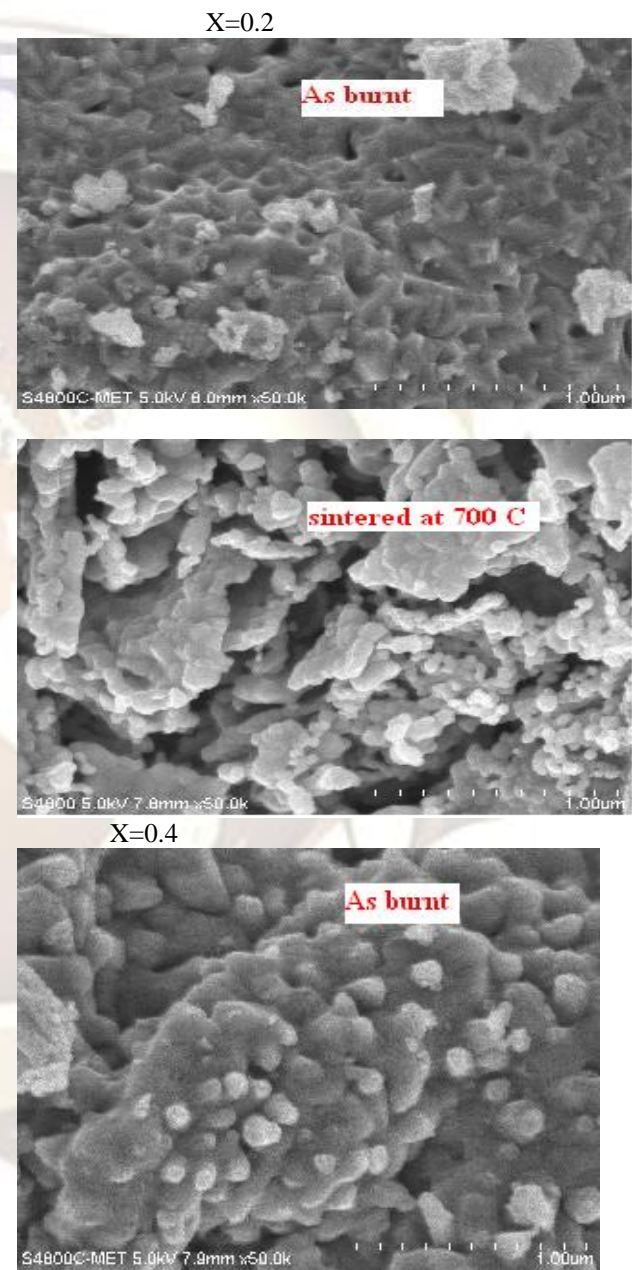




Fig. 4: SEM micrographs of $(\text{Ni}_{0.8-x}\text{Cu}_x\text{Zn}_{0.2})\text{Fe}_2\text{O}_4$ ferrite typical samples for as-burnt and the samples sintered at 700 °C.

3.3 Transmission Electron Microscopy(TEM)

The TEM images with SAED patterns for representative compound result of $(\text{Ni}_{0.8-x}\text{Cu}_x\text{Zn}_{0.2})\text{Fe}_2\text{O}_4$ ($x = 0.2, 0.4$ and 0.6) nanoparticles are shown in Fig. 5- 7. It has been observed that particles are aggregated during annealing and metal ion incorporation. The parallel lattice fringe is observed as uniformly extended over the primary building blocks, grain boundaries and pores in the samples annealed at 700° C for all compositions. Thus it can be concluded that the nanoparticles are organized in to an isooriented attached structure by sharing identical lattice planes. From selected area diffraction pattern (SAED) the corresponding planes were calculated using the relation :

$$d = \frac{\lambda L}{R} \quad (1)$$

where λ is the wavelength of electron wave, L is camera wavelength, R is radius of diffraction ring. The d values indexed in SAED pattern for each ferrite samples correlate with XRD pattern.

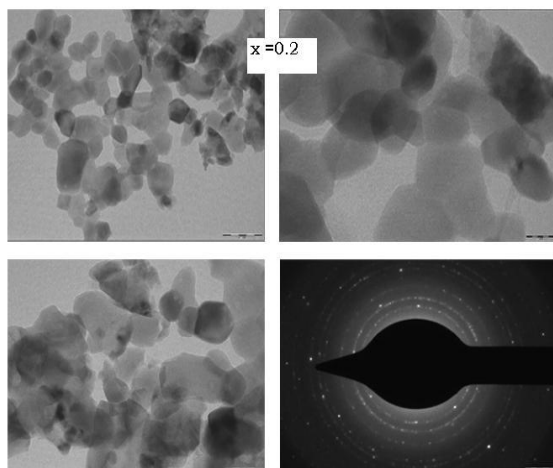


Fig. 5: TEM images for $\text{Ni}_{0.6}\text{Cu}_{0.2}\text{Zn}_{0.2}\text{Fe}_2\text{O}_4$ at 700° C.

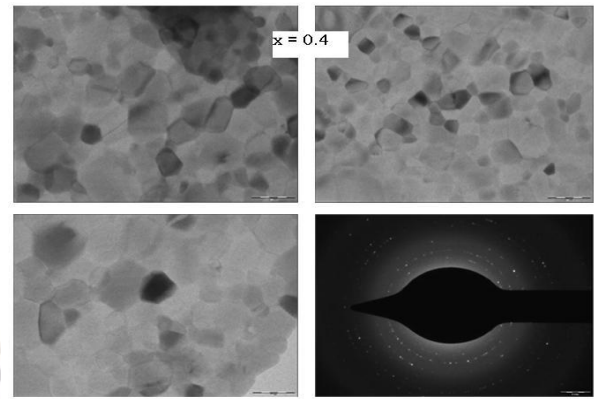


Fig. 6: TEM images for $\text{Ni}_{0.4}\text{Cu}_{0.4}\text{Zn}_{0.2}\text{Fe}_2\text{O}_4$ at 700° C.

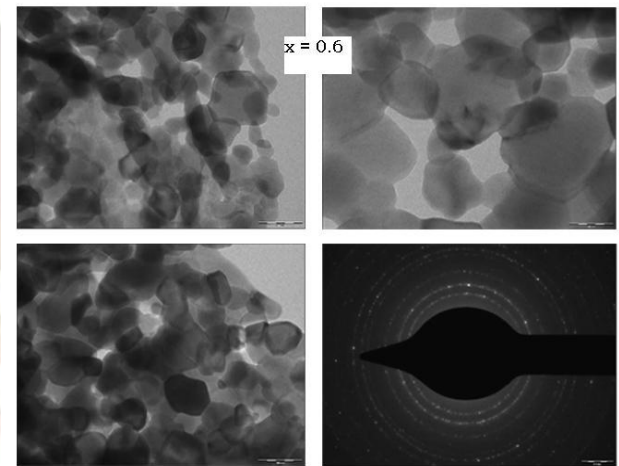


Fig. 7: TEM images for $\text{Ni}_{0.2}\text{Cu}_{0.6}\text{Zn}_{0.2}\text{Fe}_2\text{O}_4$ at 700° C

3.4 Dielectric Properties:

The dielectric constant was calculated using relation:

$$\epsilon' = \frac{Ct}{\epsilon_0 A} \quad (2)$$

Where C is the capacitance of the pellet in farad, t is the thickness of the pellet in meters, A is the cross-sectional area of the flat surface of the pellet and ϵ_0 is the constant of permittivity for free space.

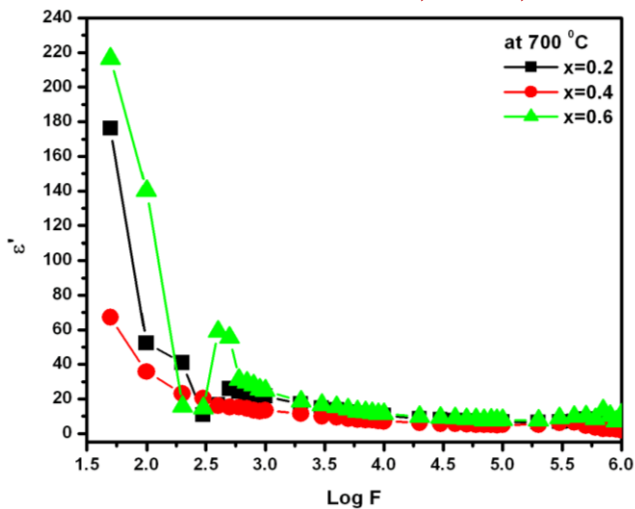


Fig. 8 : Variation of dielectric constant with frequency for $\text{Ni}_{0.8-x}\text{Cu}_x\text{Zn}_{0.2}\text{Fe}_2\text{O}_4$ ferrites with $x=0.2$ to 0.6 at 700°C .

Fig. 8 shows the variation of dielectric constant ϵ' with log frequency from 100 Hz to 1MHz and composition for samples sintered at 700°C . It can be seen that all the samples show the frequency-dependent phenomena, i.e. the dielectric constant decreases with increasing frequency exhibiting a normal ferromagnetic behavior.

All the samples reveal dispersion due to Maxwell-Wagner type interfacial polarization in agreement with Koop's phenomenological theory [36]. The higher values of dielectric constant observed at low frequencies are explained on the basis of space charge polarization due to inhomogeneous dielectric structure and resistivity of the samples[37]. The inhomoginities in the present system are impurity, porosity and grain structure.

The assembly of space charge carriers in a dielectric takes a finite time to line up their axes parallel to the alternating electric field. If the frequency of the field reversal increases, a point is reached where the space charge carriers cannot keep up with the field and the alternation of their direction lags behind that of the field as said by Chanda et al.[38]. This results in a reduction of dielectric constant of the material. Shaikh et al. [39] have quoted a similar kind of trend for dielectric constant with the change in frequency. Rabinkin and Novikova [40] pointed out that polarization in ferrites is a similar process to that of conduction. The electron exchange between $\text{Fe}^{2+} \leftrightarrow \text{Fe}^{3+}$ results the local displacement of electrons in the direction of applied field that determines the polarization. Polarization decreases with the increase in value of frequency and then reaches a constant value. It is due to the fact that beyond a certain frequency of external field, the electron exchange $\text{Fe}^{2+} \leftrightarrow \text{Fe}^{3+}$ cannot follow the alternating field. Dielectric constant ϵ' has large value at lower frequency. It is because of the predominance of species like Fe^{2+} ions, oxygen vacancies, grain boundary defects,

interfacial dislocation pile ups, voids etc [41, 42]. The decreasing trend in ϵ' with the increase in frequency is natural due to the fact that any species contributing to polarizability is found lagging behind the applied field at higher frequencies [43]. The loss factor depends upon various factors such as stoichiometry, density, grain size, Fe^{2+} content and structural homogeneity, which in turn depend on the composition and processing temperature [44].

Fig. 9 shows the variation of the dielectric loss tangent $\tan\delta$ with frequency as $\log f$ for the investigated ferrite samples. It is seen from the figure that $\tan\delta$ versus $\log f$ curves for all the samples show abnormal dielectric behavior by indicating a maximum at certain frequency. Similar types of maxima in $\tan\delta$ versus frequency have been reported for Cu-Cd [45], Li-Mg-Ti [46], Ni-Mg [47] and Mg-Zn [48] ferrite systems. The maxima are less pronounced in the investigated system than that of the reported system. The initial decrease in $\tan\delta$ with an increase in frequency may be explained on the basis of Koop's phenomenological model [36]

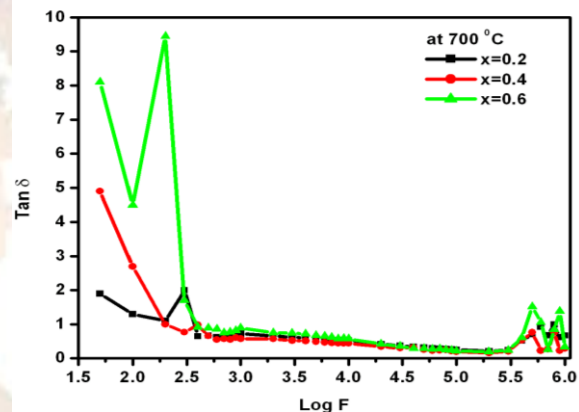


Fig.9 : Variation of loss tangent with frequency for $\text{Ni}_{0.8-x}\text{Cu}_x\text{Zn}_{0.2}\text{Fe}_2\text{O}_4$ nanoferrites with $x=0.2$ to 0.6 at 700°C .

3.5 Magnetic Properties

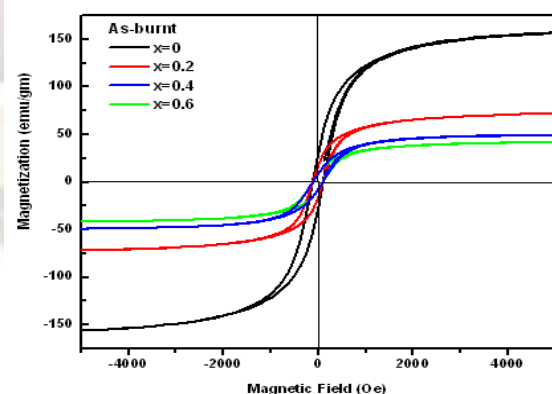


Fig.12 : Magnetic hysteresis curve for $(\text{Ni}_{0.8-x}\text{Cu}_x\text{Zn}_{0.2})\text{Fe}_2\text{O}_4$ ferrite with different Cu content measured by VSM at room temperature.

The hysteresis loops (Fig. 12) of the investigated samples were measured to determine magnetic parameters such as the saturation magnetization

(Ms) and coercivity (Hc). The measurement results are presented in Fig. 12-13, indicating that Ms decreases with the increase of Cu²⁺ substitution and as temperature increases [40]. This may be attributed to the weakening of exchange interactions due to Cu²⁺ ions. Moreover, the saturation magnetization of Ni-Cu-Zn ferrite materials is defined by their molecular magnetic moments. When Cu²⁺ ions were introduced into the Ni-Zn, they replace some of Ni²⁺ in A-site. Moreover, Cu²⁺ ions have 1 μB magnetic moment, less than 2 μB of Ni²⁺ ions. The magnetic moment in ferrite is mainly due to the uncompensated electron spin of the individual ions and the spin alignments in the two sub lattices, which are arranged in an antiparallel fashion[49].

It is clearly observed from Figs.12 and 13 that the coercivity increases as the Cu²⁺ substitution increases. The saturation magnetization is related to H_c through Brown's relation [50] :

$$H_c = \frac{2K}{\mu_i M_s} \quad (3)$$

According to this relation, H_c is inversely proportional to M_s, which is consistent with our experimental results. An increase in coercivity can also be correlated with the increase in agglomeration [51]. It may be due to the fact that due to agglomeration, various domains having different alignments come closer to each other causing an increase in magnetocrystalline anisotropy.

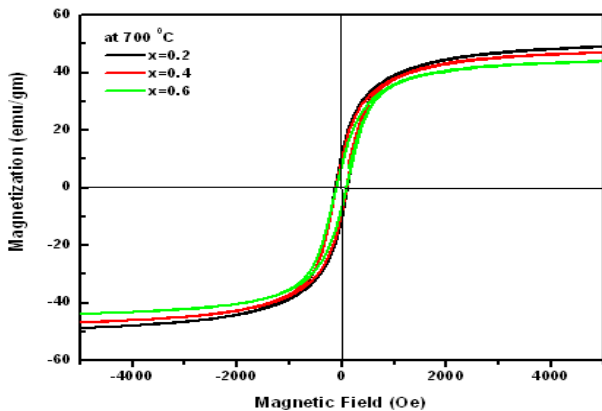


Fig.13 : Magnetic hysteresis curve for (Ni_{0.8-x}Cu_xZn_{0.2})Fe₂O₄ ferrite with different Cu content measured by VSM at 700° C.

3.6 UV characterization

Fig. 14 and Fig. 15 shows the optical absorption spectra for (Ni_{0.8-x}Cu_xZn_{0.2}) Fe₂O₄ nanocrystals in the UV region at room temperature and for the samples sintered at 700° C. There are three absorption bands observed at 227 nm, 230 nm and 232 nm in the UV-Vis spectra, which is in good agreement with the XRD results. Such absorption is related to the composition of the samples and sintering temperature as shown in Fig. 14 and Fig.

15. It is established that three types of electronic transitions occur in the optical absorption spectra of Fe³⁺ substances [52]. As it is revealed from Fig. 15 that the electronic transition for the charge transfer in the wavelength region 225-250 nm dominates for the optical absorption features of the sample while the ligand field transition in the range of 700-750 nm dominates for the optical absorption features for x= 0.2 composition. The results indicated that the sintering temperature and composition of the samples have great influence on their optical property [53].

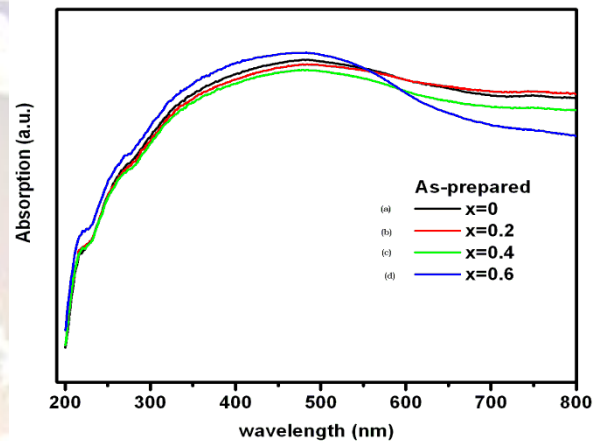


Fig.14 : UV –Vis spectra of (Ni_{0.8-x}Cu_xZn_{0.2})Fe₂O₄ nanocrystals at room temperature a) Ni_{0.8}Zn_{0.2}Fe₂O₄ (b) Ni_{0.6}Cu_{0.2}Zn_{0.2}Fe₂O₄ (c) Ni_{0.4}Cu_{0.4}Zn_{0.2}Fe₂O₄ (d) Ni_{0.2}Cu_{0.6}Zn_{0.2}Fe₂O₄

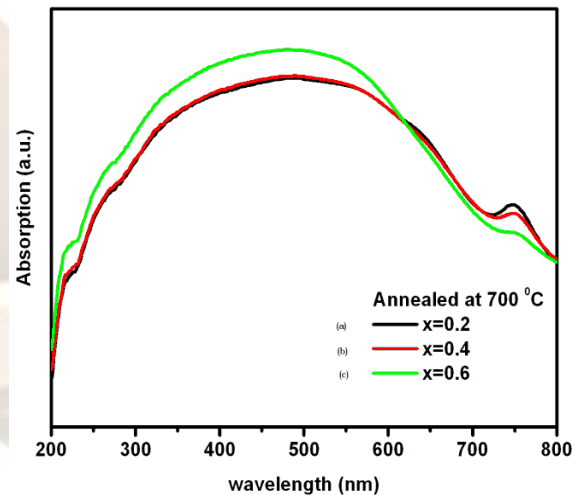


Fig.15 : UV –Vis spectra of (Ni_{0.8-x}Cu_xZn_{0.2})Fe₂O₄ nanocrystals at 700° a) (Ni_{0.6}Cu_{0.2}Zn_{0.2})Fe₂O₄ (b) Ni_{0.4}Cu_{0.4}Zn_{0.2}Fe₂O₄ (c) Ni_{0.2}Cu_{0.6}Zn_{0.2}Fe₂O₄

4. Conclusion

The auto combustion technique yields nano crystalline single phase NiCuZn ferrites. The XRD pattern shows the formation of single phase cubic spinel structure for all the samples. Lattice constant, sintered density increase whereas X-ray density,

porosity decrease with the increase in Cu concentration. The starting particle size of the composition varies from 25nm to 40 nm. Dielectric constant increases with the increase in copper concentration. This is due to the good conductivity of copper than that of nickel. Dielectric constant and dielectric loss factor both decrease with the increase in frequency and can be explained on the basis of space charge polarization. The saturation magnetization and magnetic moment decreases. The UV-Vis measurements suggest that the as prepared and sintered samples at 700° C of $Ni_{0.8-x}Cu_xZn_{0.2}Fe_2O_4$ ferrite posses different optical properties depending upon the composition of the samples. The substitution of Cu in the $Ni_{0.8-x}Cu_xZn_{0.2}Fe_2O_4$ ferrites causes appreciable changes in its structural and magnetic properties. The obtained experimental results provide important information on improving properties of NiCuZn ferrites for multilayer chip inductor application.

5. Acknowledgement

Authors would like to thank Department of Physics, University of Pune for XRD and UV, SAIF, IIT, Powai, Mumbai for SEM and TEM, CMC, National Chemical Laboratory, Pune, India for VSM, Vishay Components India Pvt. Ltd., Loni Kalbhor, Pune, India for LCR meter facilities provided. Also one of the authors V. V. Awati wish to thank BCUD, University of Pune, for the fund provided under Research Project (Proposal No. 11SCI00265).

References

- [01] H. S. Nalwa, *Magnetic Nanostructures* (American Scientific Publisher, U.S.A.2002)
- [02] Y-P Fu, C-H Lin, *J. Magn. Magn. Mater.* 251 (2002) 74.
- [03] C. Liu, B. Zou, A. J. Rondinone, Z. J. Zhang, *J. Phys. Chem. B*, 104 (2000)1141-1145.
- [04] D, K. Kim, Y. Zhang, W. Voit, K. V. Rao, *J. Magn. Magn. Mater.* 225 (2001) 30-36.
- [5] F.Li, H.Wang, L.Wang, J.Wang, *J.Magn.Magn.Mater.* 309 (2007) 295-299.
- [6] S.Sun, H.Zeng, D. B. Robinson, s. Raoux, P.M.Rice, S.X. Wang, G.Li, *J.Am.Chem.Soc.* 126 (2004) 2782.
- [7] T.Hyeon, Y.Chung, J.Park, S.S.Lee, Y.W. Kim, B.H.Park, *J.Phys.Chem. B* 106 (2002) 6831.
- [8] Q.Chen, Z.J. Zhang, *J.Appl. Phys.* 73 (1998) 3156-3158.
- [9] D. S. Mathew, R. S. Juang, *J. Chem. Engg.* 139 (2007) 51-65.
- [10] X.Niu, w.Du, *Sensor Actuators B* 99 (2004) 405-409.
- [11] N.Ikenaga, Y.Ohgaito, H. Matsushima, T.suzuki, *Fuel* 83 (2004) 661-669.
- [12] J.A.Toledo-Antonio, N.Nava, M.Martinez, X.Bokhimi, *Appl. Catal. A* 234 (2002) 137-144.
- [13] J.Qiu, C. Wang, M.Gu, *Mater.Sci. Eng. B* 112 (2004) 1-4.
- [14] G. Fan, Z. Gu, L.Yang, F.Li, *Chem.Eng. J.* 155 (2009) 534-541.
- [15] M.Kobayashi, H.Shirai, M.Nunokawa, *Ind. Eng. Chem.Res.* 41 (2002) 2903-2909.
- [16] S.Gubbala, H.Nathani, K.Koizol, R.D.K.Mishra, *J.Phys. B* 348 (2004) 317-328.
- [17] S.A.Saafan, T.M.Meaz, E.H.E1-Ghazzaway, M.K.E1Nimr, M.M.Ayad, M. Bakr, *J.Magn.Magn.Mater.* 322 (2010) 2369-2374.
- [18] S.Singhal, K.Chandra, *J.solid.State. Chem.* 180 (2007) 296-300.
- [19] C.Y.Tsay, K.S.Liu, T.F.Lin, IN.Lin, *J.Magn.Magn.Mater.* 209 (2000) 189-192.
- [20] J.C.Aphesteguy, A. Damiani, D.DiGiovanni, s.E.Jacobo, *J.Phys. B* 404 (2009) 2713-2716.
- [21] P. Bayliss, D. K. Smith, *Mineral Powder Diffraction File, JCPDS, USA* (1986)
- [22] D. Cullity, *Elements of X-ray diffraction* (Addison-Wesley Publish. Co., England (1967)) 42
- [23] Atul Thakur, P. Mathur, M. Singh, *Ind. J. Pure & Appl. Phys.* 46 (2008) 43.
- [24] S. L. Kadam, C. M. Kanamadi, K. K. Patankar and B. K. Chougule, *Mater. Lett.*, 59 (2005) 215
- [25] S. L. Kadam, K. K. Patankar, V. L. Mathe, M. B. Kothale, R. B. Kale, B. K. Chougule, *Mater. Chem. and Phys.*, 78 (2000) 178
- [26] R. P. Mahajan, K. K. Patankar, N. M. Burange, S. C. Chaudhari, A. K. Ghatage, S. A. Patil, *Indian. J. Pure and Appl. Phys.*, 38 (2000) 615-620
- [27] S. K. Kadam, K. K. Patankar, C. M. Kanamadi, B. K. Chougule *Mater. Res. Bull.*, 39 (2004) 2265-2272
- [28] M. B. Kothale, K. K. Patankar, S. L. Kadam, V. L. Mathe, A. V. Rao, B. K. Chougule *Mater. Chem. and Phys.*, 77 (2002) 691-696
- [29] E. C. Snelling (Ed), *Soft Ferrites, Properties and applications* (2nd Ed, Butter worth and Co. Ltd, London, 1988).118.
- [30] M. C. Dimri, A. Verma, S. C. Kashyap, D. C. Dube, O. P. Thakur, C. *Prakash, Mater. Sci. Engin. B* 133 (2006) 42-48.
- [31] M. U. Rana, T. Abbas, J. Magn. Magn. *Mater.* 246 (2002) 110-114.
- [32] R.S.Patil, S.V. kakatjar, S.A. Patil, A.M. Sankpla, S.R.Sawant, *Mater. Chem. Phys.* 28 (1991) 355-365.

- [33] S.S. Bellad, S.C. Watawe, A.M.Sahikh, B.K. Chougule, *Bull.Mater.Sci.* 23 (2) (2000) 83-85.
- [34] R. L. Coble, J. E Burke (Ed.), "sintering in ceramics", *Progress in ceramic Science*, vol. 3, 197.
- [35] Raming T. P, Winnubst A. J. A, Vankats, C. M. Philipse, A. P. *J. Coll. Inter. Sci*, 249, (2002) 346-350.
- [36] C. G. Koops, *Phys. Rev.* 83 (1951) 121.
- [37] A. K. Singh, T. C. Goel, R. G. Mendiratta *J. Appl. Phys.* 91 (2002) 6626-6629.
- [38] M. Chanda, Science of engineering materials, Vol. 3. *The Machmillan Company of India Ltd, New Delhi*, (1980).
- [39] A. M. Shaikh, S. S. Bellad, B. K. Chougule, *J. Magn. Magn. Mater.* 195 (1999)384.
- [40] I. T. Rabinkin, Z. I. Novikova,, *Ferrites (Izv Acad. Nauk USSR Minsk, 1960)*.
- [41] K. W. Wagner, *Ann. Phys.* 40 (1913) 817.
- [42] J. C. Maxwell, *Electricity and Magnetism vol 2* (New York, Oxford University Press, 1973).
- [43] R. G. Kharabe, R. S. Devan, C. M. Kanamadi, B. K. Chougule, *Smart Mater.Struct.* 15 (2006) N36.
- [44] A. Verma, T. C. Goel, R. G. Mendiratta, P. Kishan, *J. Magn. Magn. Mater.* 208 (2000) 13
- [45] C.B. Kolekar, P.N. Kamble, S. G. Kulkarni, A. S. Vaingankar, *J. Mater. Sci.* 30 (1995) 5784.
- [46] S.S. Bellad, B.K. Chougule, *Mater. Chem. Phys.* 66(2000) 58.
- [47] L.J. Berchamans, R. K. Selvan, P.N.S. Kumar, C.O. Augustins, *J. Magn. Magn. Mater.* 279 (2004) 103.
- [48] S. F. Manosur, *Egypt. J. solids* 28(2) (2005) 263.
- [49] A.A.Birajdar, Sagar.E.Shrisath, R.H.Kadam, S.M.Patange, K.S.Lohar, D.R. Mane, A.R. Shitre, *J.Alloy.Comp.* 512 (2012) 316.
- [50] J.M.D. Coey, *Rare Earth Permanent Magnetism* (John Wiley and Sons, New York, 1996).
- [51] M.Srivastava, A.K. Ojha, S.Chaubey, P.K.Sharma, A.C.Pandey, *Mater.Sci.Engg. B* 175 (2010) 14.
- [52] Skoog, et al. *Principles of Instrumental Analysis. 6th ed.* (Thomson Brooks/Cole. 2007), 169-173.
- [53] Gajendra K. Pradhan, K. M. Parida, *ACS Appl. Mater. Interfaces*, 2011, 3 (2), 317-323.